THE JOURNAL OF PHYSICAL CHEMISTRY B

ARTICLE

pubs.acs.org/JPCB

Proton Transfer between Tryptophan and Ionic Liquid Solvents Studied with Molecular Dynamics Simulations

Marco Klähn,* Abirami Seduraman, and Ping Wu

Institute of High Performance Computing, 1 Fusionopolis Way, #16-16, Connexis, Singapore 138632, Republic of Singapore

Supporting Information

ABSTRACT: The reaction free energies and associated pK_a values for proton transfer from positively charged tryptophan ($HTrp^+$) to the two pure ionic liquids (ILs) BMIM-PF_6 and BMIM-BF_4 are derived from molecular simulations. IL solvation effects are examined with molecular dynamics simulations together with an empirical force field in which the average charge distribution in the actual IL is taken into account. A combination of molecular mechanical and quantum mechanical description (QM/MM) is used to examine the protonation of the anion constituents of the ILs. A dissociation of the protonated anions is observed into hydrogen fluoride and BF_3 or PF_5. Finally, pK_a values of 16.5 and 21.5 in BMIM-BF_4 and BMIM-PF_6, respectively, are found for proton transfer from $HTrp^+$ to PF_6^- and BF_4^- anions, which indicates that a deprotonation of $HTrp^+$ is highly unfavorable compared to aqueous solutions. An examination of the contributions to the reaction free energies demonstrates that a deprotonation of tryptophan is impeded because two ions need to be annihilated for the reaction to occur: $HTrp^+$ and an anion. While the solvation effects induced by the two ILs are similar, the low proton acceptance of PF_6^- anions leads to the larger pK_a value in BMIM-PF_6. Also, estimates suggest that IL-induced pK_a shifts are comparably small in proton transfer reactions where the total number of ions remains unchanged. For the first time, pK_a values of acids were determined computationally in ILs. The obtained results elucidate the role of solvation effects on proton transfer between amino acids and ILs and improve our understanding of the observed pH memory of proteins that are solvated in ILs.

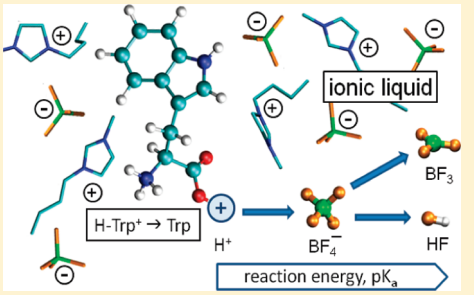

1. INTRODUCTION

Ionic liquids (ILs) are molten salts with low melting points, which in many cases were found below room temperature. Most ILs consist of organic cations, often based on imidazolium, to which alkyl chains of varying length are attached. The positive charge is delocalized over these large cations, which weakens their anion-coordination that in turn leads together with their asymmetric structure to the observed low melting points. These cations are usually paired with more compact inorganic anions, often fluoro compounds and anions that contain fluoroalkyls. ILs are characterized, among others, by nonvolatility, high viscosity, and ion conductivity as well as a high thermal and chemical stability.[1] It has been demonstrated on numerous occasions that physicochemical properties of ILs vary over a wide range of values upon independent modification of cations and anions, which makes ILs a task-specific solvent with adjustable properties. Due to the versatility of ILs, it is not surprising that a broad variety of potential applications has been suggested.[2,3]

One of the most important applications of ILs is their use as alternative adjustable solvents that are capable of solvating charged, polar and nonpolar compounds.[4,5] One solute group of particular interest are proteins and short peptide chains, and it has been observed that proteins are indeed soluble in suitable ILs, without causing protein denaturing.[6] Thus, one major application of ILs is to act as a solvent for enzymes to improve the performance of biocatalytic reactions.[7,8] Also, the utilization of ILs as protein stabilizers, for biopreservation and biosensors has been considered.[9−11] Moreover, it has been demonstrated that ILs in biphasic systems facilitate the extraction of various bioproducts, including proteins and amino acids, from an aqueous phase.[12−16] Extraction processes that involve ILs are promising because of their effectiveness and because they are environmentally more benign than conventional processes. In most of these applications, the protonation state of the biomolecules is of high importance. It has been observed, e.g., that amino acid extraction is highly sensitive to the pH value in the aqueous phase.[15] Furthermore, it is well-known that various properties of proteins depend crucially on the protonation state of their residues. The total charge of the protein highly influences its solubility in ILs for instance. Also the activity of an enzyme depends on the protonation state of the catalytic residues.[17] Finally, the protein stability is effected by the protonation state of its residues.[18] In fact, the pK_a values of residues, which determine their protonation state, have been shown to be essential parameters for the prediction of free folding energies of proteins.[19] Therefore, understanding IL induced pK_a shifts of amino acids is of major interest.

Received: March 16, 2011
Revised: May 18, 2011
Published: May 18, 2011

Studies that examine proton transfer between solutes and IL solvents are scarce. One remarkable observation is that proteins in ILs that were previously solvated in water appear to maintain the protonation state that adjusted itself according to the pH value of the water solvent. Hence, proteins in ILs appear to have a pH memory, a property that has also been found in organic solvents.[20] This observation suggests the possibility to adjust the protonation state of proteins in aqueous solution *prior* to their solvation in ILs. The underlying reason for this persistence of the protonation state in ILs, however, remains unclear. Malham et al. measured pK_a values of acetic acid, pyridinium, imidazolium, cyanophenol, ammonium, and phenol in aqueous solutions, into which the IL BMIM-BF_4 was added up to 77% of the solution volume.[21] Compared to water, a moderate increase of the pK_a values has been observed for all acids of up to 2 units with increasing IL concentration, except for ammonium, where a slight decrease of 0.07 units was observed. These pK_a increases were preceded in some cases with a slight initial decrease of the pK_a values at low IL concentrations. This trend was rationalized with a general capability of ILs to stabilize ionic species. In any event, water was still present abundantly in all investigated solutions and is thus expected to remain directly involved in the proton exchange between the acid−base pairs, considering that BF_4^- is a much weaker proton acceptor (pK_a = −4.9 in water), and $BMIM^+$ is a much weaker proton donor (p$K_a \approx 23$ in water) compared to a water molecule in the water−IL solution.[22,23] Hence, this case is fundamentally different from the situation where a solute exchanges protons with a pure IL. Thomazeau et al. used spectroscopic methods to study proton transfer reactions from protonated NTf_2, TfO and from acetic acid to nitroaniline indicator bases that were solvated by the ILs BMIM-BF_4 and BMIM-NTf_2.[24] It was observed that ILs stabilized the acids relative to the indicator bases, i.e., the acidities of the compounds were lower compared to the same proton transfer reaction in aqueous solutions. D′Anna et al. measured the pK_a shift of different benzoic acids solvated in the ILs BM_2IM-NTf_2 and BMPYR-NTf_2 with a similar method and also found a stabilization of benzoic acid relative to the probe base, with an increase of pK_a values of up to 3.5 units.[25] In both of these latter two experiments, protons were transferred between the acid and the indicator base, whose protonation can be detected with UV−vis spectroscopy. The ion constituents of the IL were not directly involved in the reaction and it is not clear how acidic the compounds would have been without the addition of the indicator bases.

The aim of this work is to assess the acidity of amino acids in pure ionic liquids, i.e. to study the proton transfer from an amino acid to IL ions, with molecular dynamics (MD) simulations. As a model case, we examine two protonation states of tryptophan, zwitterionic (Trp) and protonated ($HTrp^+$), in the two common ILs 1-butyl-3-methylimidazolium and tetrafluoroborate (BMIM-BF_4) and hexafluorophosphate (BMIM-PF_6). Even though these two ILs appear to be similar, their solvation properties differ fundamentally: while BMIM-PF_6 is water-immiscible, BMIM-BF_4 is water-miscible.[26] A comparison will clarify the influence of the anion on the acidity of Trp in the two ILs. Tryptophan is comprised of a highly polar backbone and of a hydrophobic indole moiety. This compound was chosen as an example because the solvation free energy of Trp in BMIM-PF_6 and other similar ILs relative to water is known from experiments.[15,27]

The simulations are carried out in the following sequence: In the first step, Trp and $HTrp^+$ solvated in the two ILs are simulated with classical force fields, and their solvation free energies are determined. For comparison, the solvation energies of Trp and $HTrp^+$ in water are evaluated with the same method as well. These solvation free energies are compared with measured partition coefficients of Trp and $HTrp^+$ in biphasic IL−water systems to calibrate the calculated solvation free energies. After this, the product state of the reaction is identified with MD simulations in combination with hybrid potentials, in which protonated anions are treated quantum mechanically and the solvent classically (QM/MM). Subsequently, solvation free energies of the identified products in the ILs are calculated. In the next step, the anions as well as the identified product compounds are studied in gas phase with quantum chemical methods. A combination of all these results enables the evaluation of the reaction free energy for proton transfer from $HTrp^+$ to the anions of the ILs, which are translated into pK_a values. An analysis of the composition of the reaction free energy in the last step provides insights into how these ILs influence the proton transfer reaction.

So far, only a few QM/MM simulations have been used to study chemical reactions in ILs. Acevedo et al. used a combination of the semiempirical PM3 method and classical force fields together with Monte Carlo simulations and free energy perturbation to derive free energy barriers of the Diels−Alder reaction between cyclopentadiene and acrylate in EMIM-Cl as well as a Kemp elimination reaction of benzisoxazole with piperidine in BMIM-PF_6.[28,29] For the Diels−Alder reaction, a stabilization of the transition state due to hydrogen bonds with $EMIM^+$ cations has been found, while the reproduction of a measured energy barrier in the Kemp elimination reaction was used mostly to verify a new classical force field. A halide substitution reaction of nitrobenzenesulfonate in BMIM-PF_6 was studied with a combination of semiempirical NDDO with classical force fields together with MD simulations and free energy perturbation.[30] It has been found that ILs stabilized the halide reactant states with localized charge more than the transition state with delocalized charge, which led to an increase of the free energy barrier. Finally, high energy scattering of oxygen and argon atoms from EMIM-NO_3 surfaces was investigated with semiempirical MSINDO, classical force field and MD simulations.[31] Proton transfer from cations to anions upon O and Ar impact as well as the formation of NO_2, O_2 and other compounds was observed and their occurrence probabilities were calculated.

2. METHODOLOGY

2.1. Deriving pK_a Values from Thermodynamic Cycles. For the calculation of pK_a values of amino acids (AA) in aqueous solution, the reaction free energy, ΔG_0^{aq}, for the following reaction needs to be considered:

$$HAA^+(aq) \rightarrow AA + H^+(aq) \qquad (1)$$

The direct calculation of ΔG_0^{aq} would involve substantial complications due to difficulties to calculate accurate ground state energies of the solvated reactant and products. Thus, this quantity is derived indirectly through the frequently used thermodynamic cycle (TDC) depicted in Figure 1a. The application of such a TDC reduces the problem to the calculation of the reaction free energy in gas phase, ΔG_0^{gas}. Energetically, the gas phase compounds are connected with their solvated state through solvation free energies, which can be derived with thermodynamic integration or free energy perturbation techniques. According to

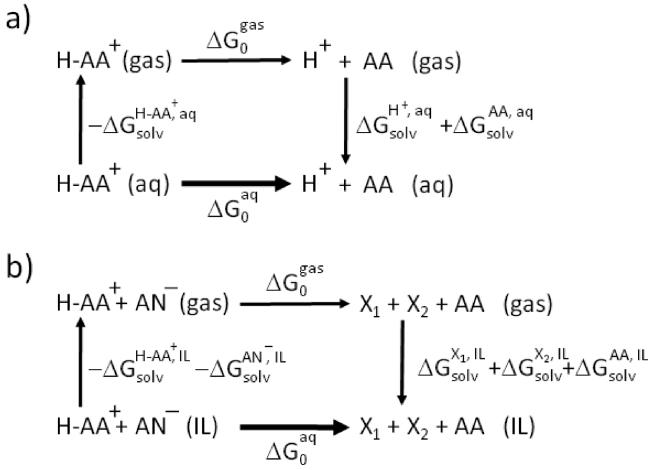

Figure 1. Thermodynamic cycle to determine the pK_a value of charged amino acids in water according to $HAA^+(aq) \rightarrow H^+ + AA(aq)$ (a) and in ILs according to $HAA^+ + AN^-(IL) \rightarrow AA + HAN(IL) \rightarrow AA + X_1 + X_2(IL)$ (b). The symbols are explained in the text.

Figure 1a, ΔG_0^{aq} can be derived as follows:

$$\Delta G_0^{aq} = -\Delta G_{solv}^{HAA^+,aq} + \Delta G_{solv}^{AA,aq} + \Delta G_{solv}^{H^+,aq} + \Delta G_0^{gas} + RT \ln V_2/V_1 \quad (2)$$

In eq 2, $\Delta G_{solv}^{HAA^+,aq}$, $\Delta G_{solv}^{AA,aq}$ and $\Delta G_{solv}^{H^+,aq}$ designate the solvation free energy of the protonated amino acid, the deprotonated amino acid and the proton in water, respectively. The last term accounts for the conversion of one mol of the reactant and product compounds, respectively, from the liquid standard state with a solute concentration of 1 M, i.e., V_1 = 1 L, to the standard state in gas phase, i.e., V_2 = 22.41 L, assuming an ideal gas.

ΔG_0^{gas} is defined as the free energy difference of products and reactants:

$$\Delta G_0^{gas} = G^{H^+} + G^{AA} - G^{HAA^+} \quad (3)$$

The computational procedure for IL solvents is quite similar. However, the situation of the proton in the product state is different. While a calculation of $\Delta G_{solv}^{H^+,aq}$ is challenging because complicated complexes of the proton with the surrounding water are formed, in the IL it can be safely assumed that the proton would protonate one of the anions, AN^-, to form the conjugate acid HAN:

$$HAA^+ + AN^-(IL) \rightarrow AA + HAN(IL) \rightarrow AA + X_1 + X_2(IL) \quad (4)$$

The actual product state in eq 4 is investigated in section 3.3, where it was found that in the ILs HAN was unstable and dissociated into two compounds, X_1 and X_2. The corresponding TDC is shown in Figure 1b, according to which ΔG_0^{IL} is calculated as follows:

$$\Delta G_0^{IL} = -\Delta G_{solv}^{HAA^+,IL} - \Delta G_{solv}^{AN^-,IL} + \Delta G_{solv}^{AA,IL} + \Delta G_{solv}^{X_1,IL} + \Delta G_{solv}^{X_2,IL} + \Delta G_0^{gas'} + RT \ln V_2/V_1 \quad (5)$$

In eq 5, $\Delta G_{solv}^{HAA^+,IL}$, $\Delta G_{solv}^{AN^-,IL}$, $\Delta G_{solv}^{AA,IL}$, $\Delta G_{solv}^{X_1,IL}$ and $\Delta G_{solv}^{X_2,IL}$ designate the solvation free energy of the protonated amino acid, an anion, the deprotonated amino acid, and the two compounds X_1 and X_2 in ILs, respectively. The gas phase reaction free energy is calculated accordingly:

$$\Delta G_0^{gas'} = G^{X_1} + G^{X_2} + G^{AA} - G^{AN} - G^{HAA^+} \quad (6)$$

In the present case, we were interested in changes of the pK_a values of amino acids in ILs relative to their well-known values in the water reference system. This comparison also enabled us to understand the calculated pK_a value changes qualitatively. Combining eqs 2, 3, 5, and 6, the reaction free energy differences, $\Delta\Delta G_0$, were calculated as follows:

$$\Delta\Delta G_0 = \Delta G_0^{aq} - \Delta G_0^{IL} = -\Delta\Delta G_{solv}^{HAA^+} + \Delta\Delta G_{solv}^{AA} + \Delta\Delta G_{solv}^{AN,IL} + \Delta\Delta G_0^{gas} \quad (7)$$

The symbols in eq 7 are defined as follows:

$$\Delta\Delta G_{solv}^{HAA^+} = \Delta G_{solv}^{HAA^+,aq} - \Delta G_{solv}^{HAA^+,IL}$$
$$\Delta\Delta G_{solv}^{AA} = \Delta G_{solv}^{AA,aq} - \Delta G_{solv}^{AA,IL}$$
$$\Delta\Delta G_{solv}^{AN,IL} = \Delta G_{solv}^{AN^-,IL} - (\Delta G_{solv}^{X_1,IL} + \Delta G_{solv}^{X_2,IL})$$
$$\Delta\Delta G_0^{gas} = \Delta G_{solv}^{H^+,aq} - ((G^{X_1} + G^{X_2}) - (G^{H^+} + G^{AN})) \quad (8)$$

The first two terms in eq 7 describe the change of solvation energy upon transferring the protonated and deprotonated amino acid from water to the IL, respectively. The third term contains the difference in solvation energy of the anion and the decay products of the conjugate acid in the IL. The last term compares the solvation free energy of a proton in water with the free energy that is released by protonating the anion in gas phase. Both of these contributions can be seen as the binding energy of the proton to its environment, which is a cluster of water molecules in aqueous solution and the decay products of the protonated anion in the latter case. The shift of the pK_a value in the IL, compared to water, is then given by

$$\Delta pK_a = pK_a^{aq} - pK_a^{IL} = \frac{\Delta\Delta G_0}{RT \ln 10} \quad (9)$$

In this equation, T designates the temperature and R is the gas constant. This means that for the evaluation of the pK_a shift, the solvation free energies of the protonated and deprotonated amino acids in water and ILs need to be calculated. Furthermore, the solvation free energies in ILs and ground state free energy in gas phase of the anions and of the decay products of their conjugate acids need to be derived. The values of pK_a^{IL} can be determined in the last step by using the experimentally well-known values of pK_a^{aq}.

2.2. Free Energy of Ground States in Gas Phase. The ground state energies of anions and product state compounds were calculated with the software Gaussian 03.[32] The geometries were optimized using second order Møller−Plesset perturbation (MP2) in combination with a triple-ζ 6-311++G(d,p) basis set.[33] The free energy, G, of the compounds was calculated as follows:

$$G = H - TS_{tot} = E_{tot} + k_B T - TS_{tot} = E_0 + E_{ZP} + E_{therm} + k_B T - TS_{tot} \quad (10)$$

In eq 10, H designates enthalpy, T is temperature, S is entropy, and k_B is the Boltzmann constant. The zero-point vibrational energy,

dx.doi.org/10.1021/jp202486j |J. Phys. Chem. B 2011, 115, 8231–8241

E_{zp}, and a thermal energy correction, E_{therm}, are added to the electron ground state energy, E_0, to yield E_{tot}.[34] For the calculation of E_{therm} and S_{tot}, all translational, rotational, vibrational, and electronic degrees of freedom were considered, in accordance with the standard procedure used in Gaussian. Entropy and thermal corrections were calculated at 300 K.

2.3. Calculation of Solvation Free Energies with MD Simulations. Solvation free energies were calculated with GROMACS, using thermodynamic integration.[35] In these simulations the interactions between solute and solvent are gradually switched off. In MD simulations, the following potential, $E(\lambda)$, is used:

$$E(\lambda) = (1-\lambda)E_{\mathrm{Tot}} - \lambda E_{\mathrm{Tot\text{-}sS}} \qquad (11)$$

In eq 11, E_{Tot} and $E_{\mathrm{Tot\text{-}sS}}$ designate the complete potential energy and the potential in which all interactions between solute and solvent are ignored, respectively. The parameter λ is increased stepwise from 0 to 1. Then the solvation free energy is derived from integration of the thermodynamic force:

$$\Delta G_{\mathrm{solv}} = \int_0^1 \left\langle \frac{\partial E}{\partial \lambda} \right\rangle_{\mathrm{MD\ \ with\ \ } E(\lambda)\mathrm{d}\lambda} \qquad (12)$$

Values of $\partial E/\partial\lambda$ at a particular value λ_i, the λ-points, are calculated as averages from MD simulations that used the corresponding potential $E(\lambda_i)$. For the numerical integration of eq 12, the Simpson's rule method was applied.

In the first step of the simulations only the Coulomb interactions between solute and solvent were switched off. The simulations started from equilibrated systems, whose preparation will be described in the next sections. Subsequently, in the second step, the remaining Lennard-Jones interactions were switched off. Both contributions together constitute the solvation free energy of the solute. A soft-core potential was used to avoid singularities in the potential energy at λ close to 1. The standard soft-core potential implemented in GROMACS was used with the parameters $\alpha = 0.5$, $\sigma = 3$ Å, and a λ-exponent of 1.[36] Values of λ were increased stepwise from 0 to 1 using a step width of $\Delta\lambda = 0.1$. In regions of larger λ-gradients, a finer step width of 0.05 was used instead. Simulations of 500 ps length were performed at each λ-point, resulting in a total simulation length of at least 11 ns for each system. For the error analysis we used the block averaging technique at each λ-point and error propagation to determine the statistical uncertainty of ΔG_{solv}.[37]

For improved statistics, the interactions of 10 solutes in the solvent were switched off simultaneously, and the average solvation free energy per solute was calculated. Simulation boxes were chosen to be sufficiently large, so that interactions among solutes were negligible compared to solute−solvent interactions. Thus, the calculated values of ΔG_{solv} approached the limit of infinitely diluted solutes. This assumption was scrutinized for one test case, $HTrp^+$ solvated in BMIM-PF_6, where only one solute was added to the solvent. The solvation free energies of this solute in 10 different replicas of the simulation are listed in the Supporting Information in Table S1, together with the average value. The latter value was compared with the case where 10 $HTrp^+$ solutes were added to the solvent and for which the solvation free energy was calculated by decoupling all solutes simultaneously from the solvent. A deviation of only 1.1 kcal/mol was found, which corresponds to about 1% of the solvation free energy. This demonstrates that interactions among solutes indeed remained negligible and that the computationally much less demanding approach where the solvation free energy of 10 solutes was evaluated simultaneously is applicable.

Table 1. Force Field Parameters for BF_3, PF_5, and HF [a]

bond potential			angle potential		
	l_0 [Å]	k_{ij} [kJ/(Å^2·mol)]		φ_0 [deg]	k_{ijk} [kJ/mol]
B−F	1.32	3235	F−B−F	120.0	670
P−F_1	1.56	3100	F_1−P−F_1	120.0	1165
P−F_2	1.60	3100	F_1−P−F_2	90.0	1165
F_H−H	0.92	3267	F_2−P−F_2	180.0	1165

Lennard-Jones Potential		
	σ[Å]	ε[kJ/mol]
B	3.58	0.3975
P	3.74	0.8368
F	3.12	0.2552
H	0	0

[a] The used atom type names are explained in Figure 2. Other symbols refer to the designations used in eq 1 of ref 38.

2.4. Specification of Force Fields. All compounds in this work were described with an empirical molecular mechanical (MM) force field that uses the standard functional form as described, e.g., in ref 38. In solvents such as ILs and water, the dominant contribution to the solvation energy originates from solute−solvent Coulomb interactions. Therefore, special care was taken throughout this work to develop a force field that is adequate to describe the electrostatics in these solutions. The force field for the ILs is based on the parametrization of Lopes et al.[39] However, the electrostatic description was refined in our preceding work and does not rely on isolated ions or ion pairs to represent the electrostatics in the IL.[26,38] The partial charges that were assigned to ions in BMIM-BF_4 and BMIM-PF_6 can be found in Figure 1 of ref 26.

For the parametrization of BF_3, PF_5, and HF, which are the compounds that comprise X_1 and X_2 that were introduced in section 2.1, equilibrium bond lengths and angles were derived from optimized gas phase structures, using density functional theory (DFT) with the B3LYP hybrid functional and a 6-31+G(d) basis set.[40,41] Force constants for bond and angle vibrations were approximated with corresponding parameters from BF_4^- and PF_6^-. The average charge distributions of BF_3, PF_5, and HF, solvated in the two ILs, respectively, were determined using a combined quantum mechanical/molecular mechanical (QM/MM) approach, in which one BF_3, PF_5 or HF compound was described with DFT, while the rest of the IL was described with the classical force field. For all QM/MM calculations in this work, the coupling of the MD software GROMACS with Gaussian using the electronic embedding approach was used.[35,42] This approach takes into account the polarization of the solute charges that are induced by the electrostatic potential of the solvent. The corresponding QM/MM potentials were minimized, and for the resulting charge distribution, partial charges were derived with the CHELPG scheme that reproduce the electrostatic potential of the original charge distribution (ESP charges).[43] This procedure was repeated for a sample of 10 different starting structures of the compounds, respectively. The partial charges were averaged over these samples and subsequently substituted as parameters into the force field. Details of this procedure are described in

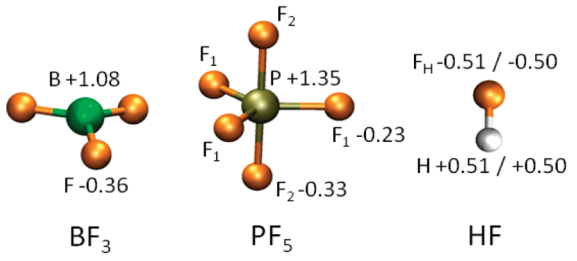

Figure 2. Liquid phase partial charges of BF_3 in BMIM-BF_4, PF_5 in BMIM-PF_6, and HF in BMIM-BF_4 and BMIM-PF_6, respectively. These partial charges reproduce the electrostatic potential of the compounds in the actual liquid phase of the simulated ILs and were derived with a QM/MM approach. Partial charges are given as fractions of the elementary charge.

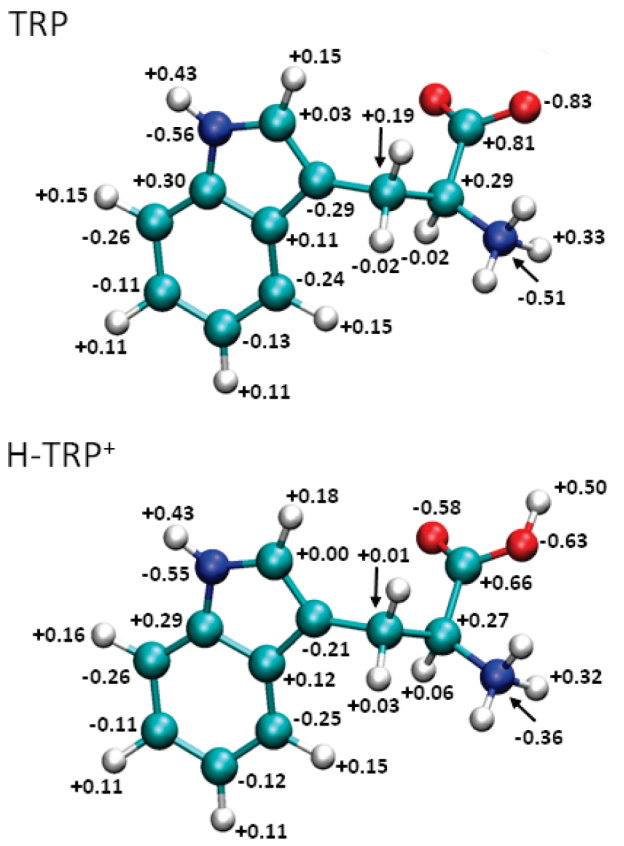

Figure 3. Liquid phase partial charges of the zwitterion amino acid Trp and protonated H-Trp^+ solvated in water. These partial charges reproduce the electrostatic potential of the compounds in water and were derived with a continuum model for water. For chemically equivalent atoms, only the average partial charge is shown. Partial charges are given as fractions of the elementary charge.

ref 38. The full set of force field parameters for these compounds is shown in Table 1 and Figure 2.

Protonated and zwitterionic tryptophan were described with the widely used AMBER03 force field.[44] Again, the partial charges were refined according to the charge distribution of Trp solvated in ILs and water to account for charge polarization induced by the solvents. For Trp in water, partial charges were derived from DFT calculations with the method mentioned above, while water was described with a polarizable continuum

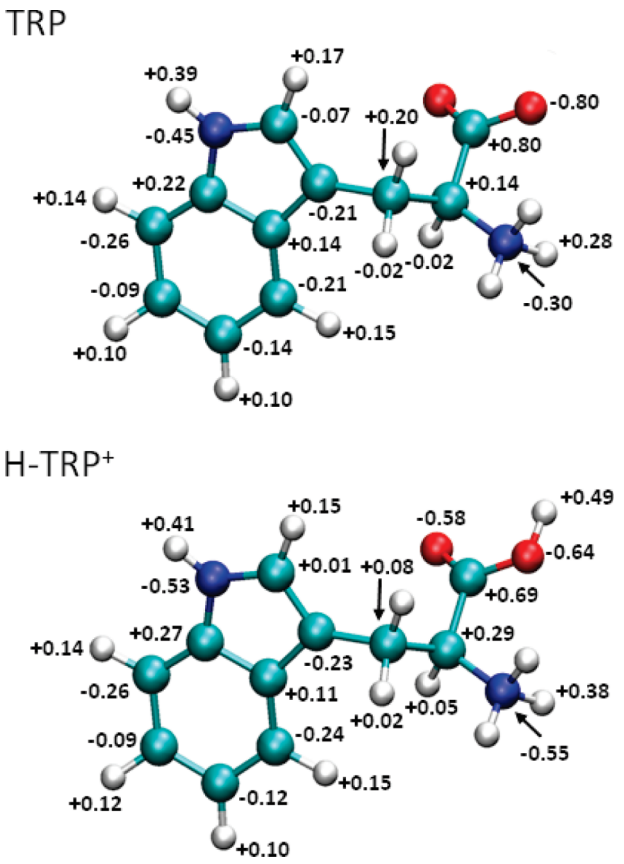

Figure 4. Liquid phase partial charges of the zwitterion amino acid Trp and protonated H-Trp^+ in BMIM-BF_4. These partial charges reproduce the electrostatic potential of the compounds in the actual liquid phase of the simulated IL and were derived with a QM/MM approach. For chemically equivalent atoms, only the average partial charge is shown. Partial charges are given as fractions of the elementary charge.

model (PCM).[45] After a geometry optimization the partial charges were derived with the CHELPG scheme and are shown in Figure 3. For the solvation in ILs, the average partial charges of Trp in the solvent were derived with the QM/MM approach described above, and the results are shown in Figure 4. The charge distribution of Trp in BMIM-PF_6 is very similar and is therefore not shown.

Water was described with the commonly used TIP5P model, where the two electron lone pairs of the water oxygen atoms are represented by two dummy atoms, respectively, onto which the partial charge of the oxygen atom is transferred.[46,47]

2.5. Characterization of MD Simulations. All MD simulations were performed with the simulation software GROMACS.[35] For simulations of Trp and $HTrp^+$ in water, 10 solutes were solvated with 2700 water molecules in a cubic box of about 44 Å box length, respectively. Furthermore, 10 residues Trp and $HTrp^+$ were solvated in BMIM-BF_4 and BMIM-PF_6 in simulation boxes that contained 490 ion pairs, respectively. The simulation box lengths were about 54 Å and 56 Å after equilibration, respectively. However, the initial box dimensions were chosen to be larger to obtain a dilution of the ILs of about a factor of 2 compared to measured densities to increase the initial ion mobility. All simulations contained between 14 000 and 16 000 atoms.

Hydrogen atoms were treated explicitly, and no degrees of freedom were constrained during the simulations. Nonbonded

interactions were calculated explicitly up to a cutoff radius of 15 Å. The fast particle-mesh Ewald summation and dispersion energy corrections were used to account for long-range Coulomb and van der Waals interactions.[48−50] Full periodic boundary conditions were applied. In the first step, initial close contacts between compounds were removed by minimizing the corresponding potential energy with the conjugate gradient method. Subsequently, the systems were equilibrated in the isothermal−isobaric (NPT) ensemble, in which temperature was controlled with the stochastic velocity rescaling method and pressure with Berendsen coupling.[51,52] The coupling time constants used for the thermostat and barostat were 0.1 and 1 ps, respectively. The compressibility and target pressure of the barostat were 4.5×10^{-5} bar^{-1} and 1 atm, respectively. Free energy MD simulations were performed in the isothermal−isochoric (NVT) ensemble. The integration step size of all MD simulations was 1 fs. For simulations with water, the target temperature was linearly increased to 300 K during the first 100 ps. Subsequently, the simulations were continued for another 400 ps at a constant temperature of 300 K. For simulations in ILs, the system was heated up to 600 K during the first 100 ps. The simulations were continued for 900 ps at 600 K. In the next step, partial charges of Trp and $HTrp^+$ were refined with the QM/MM approach described in section 2.4. The simulations were then continued for another 500 ps at 600 K and were cooled down linearly to 300 K during the following 100 ps. The systems were subsequently equilibrated at 300 K for 1 ns. The initial heating of ILs up to 600 K was necessary to facilitate ion mobility, which prevents ions from being trapped in energetically unfavorable positions close to their arbitrary initial positions. Keeping in mind the notorious low diffusivity in ILs at 300 K, these measures were particularly advantageous. These equilibrated simulations were then used to initialize solvation free energy MD simulations.

QM/MM MD simulations were performed to study the product state of the proton transfer reaction. In these simulations a proton together with three surrounding anions from the IL was described with DFT. Atom positions were initialized with structures taken from previously equilibrated IL systems to which protons were added as charged point masses, as explained in section 3.3. The B3LYP functional and a 6-31+G(d) basis set were used together with the software Gaussian to describe the DFT fragment. The remaining part of the system, the MM fragment, was treated with the force field described in the previous section. The same QM/MM coupling was used as described in 2.4 (see also ref 38). MD simulations were carried out with GROMACS similar to the other classical simulations by integrating the classical atomic equations of motion. In this approach, atomic forces are composed of contributions from the MM fragment, which are derived from the force field, and forces that stem from the DFT fragment, which are calculated directly from the electron distribution (see, e.g., ref 53 for details). The integration step size of these MD simulations was 0.5 fs. One thousand integration steps were performed, which resulted in a total simulation length of 0.5 ps. QM/MM MD simulations were performed in the isothermal-isochoric (NVT) ensemble.

3. RESULTS AND DISCUSSION

3.1. Solvation of Tryptophan and Proton in Water. In the first step, the solvation energies of Trp and $HTrp^+$ in water were calculated. Values of $\langle \partial E/\partial \lambda \rangle$ at different λ-points for the Coulomb and van der Waals contributions, respectively, are shown in Figure S1 (Supporting Information). The corresponding solvation free energies are listed in Table 2. The solvation free energy values of −80 and −58 kcal/mol for $HTrp^+$ and Trp, respectively, demonstrate that both protonation states are well solvated in water. Trp is a zwitterion and contains a negatively charged COO^- and a positively charged NH_3^+-group, whose solvation is expected to contribute most to the total solvation energy of Trp.

Table 2. Solvation Free Energy and Contributions from Coulomb and van der Waals Interactions of Protonated $HTrp^+$ and Trp in Water[a,b]

solute	ΔG^{aq}_{solv}	$\Delta G^{aq}_{solv,Coul}$	$\Delta G^{aq}_{solv,vdW}$
$HTrp^+$	-79.6_1	-78.8_1	-0.74_6
Trp	-57.6_1	-56.9_1	-0.73_6

[a] All values are given in kcal/mol. [b] Statistical uncertainties of the last digit are given as subscripts.

Table 3. Solvation Free Energy and Contributions from Coulomb and van der Waals Interactions of Water in BMIM-PF_6 as a Function of the Simulation Time per λ-Step[a,b]

simulation time [ps]	ΔG^{IL}_{solv}	$\Delta G^{IL}_{solv,Coul}$	$\Delta G^{IL}_{solv,vdW}$
50	-5.4_1	-7.2_1	1.8_1
100	-5.2_1	-6.9_1	1.7_1
200	-5.0_2	-6.8_1	1.7_1
500	-4.8_1	-6.6_1	1.8_1
800	-4.6_1	-6.5_1	1.87_3

[a] All energies are given in kcal/mol. [b] Statistical uncertainties of the last digit are given as subscripts.

In the case of Trp, two groups reported solvation free energies from simulation studies: Chang et al. reported a value of −64.6 kcal/mol, while Vöhringer-Martinez et al. calculated a value of −61.5 kcal/mol.[54,55] The latter group argued that Chang et al. probably overestimated the solvation energy because a small box of only 20 Å length was used for simulations. Due to periodic boundary conditions, artificial interactions of Trp with its own periodic images would significantly contribute to the solvation energy at such short distances, given the large size of Trp, thus leading to the assumed overestimation. We agree with this argument and like to add that Chang et al. found for Trp the largest solvation energy compared to 14 other uncharged amino acids, for which values varied between −54.4 (threonine) and −61.6 kcal/mol (tyrosine) otherwise. Considering the hydrophobic side chain of Trp, it seems implausible that the solvation of Trp would be more favorable in water than that of glutamine for instance. Therefore, we prefer to compare our result with the value from ref 55. The significant difference of 3.9 kcal/mol is most likely due to the different force fields that were used. The OPLS-AA and TIP4P force fields were used in ref 55 for Trp and water, respectively.[56] In our case, the AMBER force field with refined liquid-phase charge distribution and the TIP5P model were used instead. Unfortunately, the solvation energy of Trp has not been measured experimentally. Hence, it is presently not possible to decide which value is closer to the actual value.

For the proton solvation energy, $\Delta G^{H^+,aq}_{solv}$, we use an experimentally determined value, since a computational evaluation is quite challenging and would require an extensive ab initio model of large water clusters.[57] Instead, we rely on the value

Table 4. Comparison of Calculated Scaled Solvation Free Energies with Measured Solvation Free Energies

solute−solvent[a]	ΔG_{solv}^{theo}[b] [kcal/mol]	ΔG_{solv}^{exp} [kcal/mol]
$HTrp^+$−BMIM-PF_6	−81.6	∼ −79.6[c]
$HTrp^+$−C8MIM-PF_6	−78.6	> −79.6[c]
$HTrp^+$−C8MIM-BF_4	−82.6	< −79.6[c]
Trp−BMIM-PF_6	−55.5	> −57.6[c]
H_2O−BMIM-PF_6	−3.8	−3.9[d]

[a] ILs that contained amino acids were saturated with water according to measured saturation concentrations. [b] Calculated solvation free energies were scaled with a factor of 0.80. [c] Range of values were derived from measured partition coefficients of tryptophan in biphasic systems with water from ref 15 and 27 and from calculated solvation free energies of tryptophan in water according to Table 2. [d] Value was taken from ref 60.

of −264.23 kcal/mol that was derived from a set of cluster-ion solvation measurements.[58] This value was also confirmed by more recent first-principle calculations.[59]

3.2. Solvation of Tryptophan in ILs. Prior to the solvation of tryptophan, the solvation of water molecules in BMIM-PF_6 was considered first to scrutinize our method to derive solvation energies in ILs. A solvation free energy of −3.9 kcal/mol for water was measured by Anthony et al. for this IL.[60] In simulations, we increased the simulation length from 50 ps stepwise to 800 ps per λ-point to examine how sensitive the calculated solvation energy is to the simulation length. The obtained values are listed in Table 3. With increasing simulation time the calculated solvation energy approached the measured value. However, these results also indicate that a full convergence has not been achieved even after 800 ps, which corresponds to a total simulation length of 17.6 ns. While the van der Waals contribution converged after short simulation times, a full convergence of the Coulomb contribution seems to require total simulation times that substantially exceed 1 ns per λ-point. The reason behind this convergence problem is the slow reorganization of the IL upon changes in the electrostatic potential. For thermodynamic integration or free energy perturbation methods, the Coulomb interactions between solute and solvent are gradually changed, which causes the IL solvent to reorganize around the solute accordingly. In water for instance, this reorganization process is usually completed within picoseconds. In ILs, however, reorganization is massively impeded because the constituting ions are highly organized in an alternating pattern of cations and anions. Therefore, a reorganization of the ions in the vicinity of the solute would also involve a reorganization of surrounding solvation shells. This strong long distance correlation of ion positions together with low ion mobility in ILs led to very slow reorganization times of the solvent. Simulation times that would fully overcome this problem are unfortunately computationally prohibitively expensive, considering that several such simulations were required for this work. The measured solvation free energy of water is a factor of 0.81 smaller than the calculated value with a simulation time of 500 ps per λ-point. Keeping this deviation in mind, we proceeded with a comparison of calculated solvation energies of Trp in ILs with experimental data.

The partition coefficients of Trp between water and BMIM-PF_6 have been measured as a function of the pH value in water.[15,27] At a pH between 2.4 and 9.3, Trp is mostly zwitterionic in water. Partition coefficients are defined as the ratio of Trp concentration in the IL and the water phase. A value below 0.02 at pH > 4 indicates that Trp is solvated almost exclusively in the water phase, i.e., the solvation of Trp in water is more favorable than in the IL. For pH values around 1, most Trp are protonated to form $HTrp^+$. In that case, partition coefficients between 0.4 and 0.45 have been measured. The data also strongly suggest that the partition coefficients approach a value between 0.5 and 1 at pH < 1 (see Table 4 in ref 15). This means that $HTrp^+$ is partitioned between water and the IL in comparable amounts. This indicates that the solvation free energies of $HTrp^+$ in water and in the IL are similar. Calculated solvation free energies of Trp and $HTrp^+$ in BMIM-PF_6 were found to be −69.4 and −102.0 kcal/mol, respectively. In these simulations, 168 water molecules were added to the IL, which corresponds to the water saturation concentration in BMIM-PF_6.[61] The addition of water was necessary to enable a direct comparison with the experimental situation, where BMIM-PF_6 was brought into direct contact with water. In such biphasic systems there is sufficient time for water to diffuse into the IL until saturation is reached. A comparison with the calculated solvation energies of Trp and $HTrp^+$ in water from Table 2 shows that the calculated solvation energies in ILs are overestimated compared with the corresponding values in water. Considering the discussion above, this was not unexpected. The solvation energy of Trp suggests an overestimation of >17%, while the solvation energy of $HTrp^+$ indicates an overestimation of ∼22%. The same comparison of calculated solvation energies with measured partition coefficients for $HTrp^+$ solvated in the two ILs C8MIM-PF_6 and C8MIM-BF_4, where exactly the same simulation methods were used, led to the same conclusion that solvation energies in ILs were overestimated between 19 and 23%, which will be described in detail in a subsequent work. All these findings are consistent and suggest a constant scaling factor of 0.80 for solvation energies in ILs. Such scaling reproduced all experimental results regarding measured partition coefficients as well as the directly measured solvation free energy of water in BMIM-PF_6. The comparison of scaled solvation energies with experimental data is summarized in Table 4. These results are encouraging and thus a scaling factor of 0.80 was adopted and applied in the following to all calculated solvation energies in ILs. A scaling of solvation energies in water was not necessary, since solvent reorganization occurs on much shorter time scales in these cases.

Table 5. Solvation Free Energy and Contributions from Coulomb and van der Waals Interactions of Protonated $HTrp^+$ and Trp in ILs[a,b,c]

solvent	solute	ΔG_{solv}^{IL}	$\Delta G_{solv,Coul}^{IL}$	$\Delta G_{solv,vdW}^{IL}$
BMIM-PF_6	$HTrp^+$	$\mathbf{-70.6_2}$	-62.6_2	-8.0_1
	Trp	$\mathbf{-39.9_2}$	-32.1_2	-7.8_1
BMIM-BF_4	$HTrp^+$	$\mathbf{-75.2_3}$	-67.8_2	-7.4_1
	Trp	$\mathbf{-42.4_2}$	-35.5_2	-6.9_1

[a] All values are given in kcal/mol. [b] Solvation energies were scaled with a factor of 0.80 as explained in section 3.2. [c] Statistical uncertainties of the last digit are given as subscripts.

The solvation free energies of Trp and $HTrp^+$ in the two pure ILs BMIM-PF_6 and BMIM-BF_4 have been calculated and the results are listed in Table 5, while values of $\langle \partial E/\partial \lambda \rangle$ are shown in Figures S2 and S3. The solvation of $HTrp^+$ and Trp is less favorable in both ILs compared to water. In the case of $HTRP^+$, solvation energies increased 9 and 5 kcal/mol in BMIM-PF_6 and BMIM-BF_4, respectively, and for Trp values increased 18 and 16 kcal/mol in BMIM-PF_6 and BMIM-BF_4, respectively. The

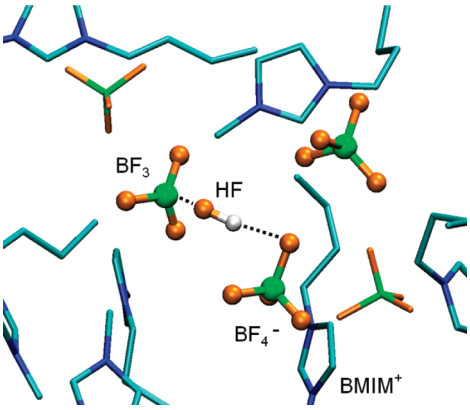

Figure 5. Representative structure of HBF_4 in BMIM-BF_4 as derived from QM/MM MD simulations. Two anions and HBF_4 were described with DFT (shown in the ball and stick representation), while the remaining part of the system was described with an empirical force field. All ions in the vicinity of the DFT fragment are displayed, where hydrogen atoms were omitted to improve clarity. It was observed that HBF_4 dissociated into BF_3 and HF, where the latter compound formed strong hydrogen bonds with BF_3 as well as with one of the anions.

unfavorable solvation of Trp in the two ILs is probably due to the large solute cage formation energies in ILs, where the accommodation of amino acids in the solvent requires the separation of several coordinated counterions.[62] This effect is partially compensated in the case of $HTrp^+$, where the additional charge is stabilized by the ions in the IL. Solvation of tryptophan is improved when BF_4^- anions are involved, compared to PF_6^-, which is also in line with measured partition coefficients.[15,27] This can be explained with the larger anion surface charges in the case of BF_4^-. Larger negative partial charges on the fluorine atoms account for stronger hydrogen bonds between BF_4^- and the solute. The concept of ion surface charge to estimate IL−solute interaction strengths has also been applied successfully in a previous work to water−IL mixtures.[26] It should also be mentioned that the solvation of $HTrp^+$ in the two studied ILs becomes more favorable than in water when the ILs are saturated with water. This enables the extraction of amino acids with ILs from aqueous solutions in biphasic systems, as observed in experiments.

3.3. Solvation of Anions before and after Protonation in ILs. In this part the solvation energies of the anions BF_4^- and PF_6^- as well as those of the corresponding protonated product states were derived. While this is straightforward in the case of the anions, the product states required additional considerations. The way in which protons bind to ions after their transfer from $HTrp^+$ to the IL needs to be clarified. Apparently, the proton will strongly interact with the anions. However, it is not clear, whether one anion will simply accept the proton to form HPF_6 or HBF_4, or if the proton will associate with several anions to form a larger complex, similar to the situation of protons in water. Another possibility is that the protonated anions dissociate into other compounds.

Ten protons were added to the simulations of pure BMIM-PF_6 and BMIM-BF_4 to answer this question. In the first step, these protons were treated simply as point charges with the mass of a proton, a charge of +1 *e* and the Lennard-Jones parameters of a $BMIM^+$-hydrogen atom. These parameters were only used in the first step to generate initial proton positions with classical MD simulations of 1 ns length. Resulting structures were used in the second step to initialize more realistic QM/MM MD simulations using the approach described in section 2.5. According to the classical MD simulations, protons were coordinated to three anions in most cases. In successive QM/MM simulations, the proton was described together with the three coordinating anions with DFT, while the remaining part of the system was described with the empirical force field, which is explained in section 2.5. Three such QM/MM MD simulations with different starting structures were performed for BMIM-PF_6 and BMIM-BF_4, respectively.

Table 6. Solvation Free Energy and Contributions from Coulomb and van der Waals Interactions of Anions and their Decay Products after Protonation in ILs[a,b,c]

solvent	solute	ΔG^{IL}_{solv}	$\Delta G^{IL}_{solv,Coul}$	$\Delta G^{IL}_{solv,vdW}$
BMIM-PF_6	HF	-2.23_8	-4.05_5	1.81_7
	PF_5	-1.2_1	-1.20_7	0.02_7
	PF_6^-	-39.9_2	-39.9_3	0.06_7
BMIM-BF_4	HF	-2.53_5	-4.62_4	2.10_3
	BF_3	-0.6_1	-2.0_1	1.4_1
	BF_4^-	-40.8_2	-42.2_2	1.3_1

[a] All values are given in kcal/mol. [b] Solvation energies were scaled with a factor of 0.80 as explained in section 3.2. [c] Statistical uncertainties of the last digit are given as subscripts.

In all these six QM/MM simulations, the protons dissociated one fluorine atom from one of the anions to form hydrogen fluoride, which readily formed within the first 5−10 fs of the simulations. These HF compounds remained stable throughout the remainder of the simulations in most cases. In all the other cases, the abstracted fluorine atom was returned to the anion, and HF was immediately formed with another anion. This means that in all QM/MM simulations, at all times, the additional protons were part of dissociated HF. These HF molecules remained associated with the remaining BF_3 or PF_5 molecules, while typically a strong hydrogen bond between HF and a second anion was formed. A representative structure of the QM fragment is shown in Figure 5. The structure of BF_3 is planar, while PF_5 is trigonal bipyramidal, where three equatorial fluorine atoms form one plane (F_1 in Figure 2) onto which the connection of two axial fluorine atoms (F_2 in Figure 2) is perpendicular.

While the QM/MM MD simulations clearly demonstrated the instability of HBF_4 and HPF_6, the simulation times were not sufficient to explore the stability of the obtained complexes $HF \cdot BF_3$ and $HF \cdot PF_5$. Therefore, classical MD simulations with an MM force field for BF_3, PF_5, and HF as specified in section 2.4 were conducted at 300 K, which were initialized according to the final structures of the QM/MM MD simulations, with $HF \cdot BF_3$ and $HF \cdot PF_5$ solvated in the corresponding ILs, respectively. After simulations of 5 ns length, 6 and 7 out of 10 $HF \cdot BF_3$ and $HF \cdot PF_5$ complexes, respectively, dissociated and diffused separately as BF_3, PF_5, and HF compounds in the solvent. According to these results it seems that eventually, after sufficiently long simulation times, all complexes would dissociate within tens of nanoseconds. Therefore, for the product state of the proton transfer reaction, BF_3, PF_5, and HF were considered as independent solutes. BF_3 and HF as well as PF_5 and HF are the compounds designated as X_1 and X_2 in eq 4, respectively.

The solvation free energies of these compounds and the corresponding anions are given in Table 6. Values for $\langle \partial E/\partial \lambda \rangle$ are shown in Figures S4 and S5. The solvation energies of the

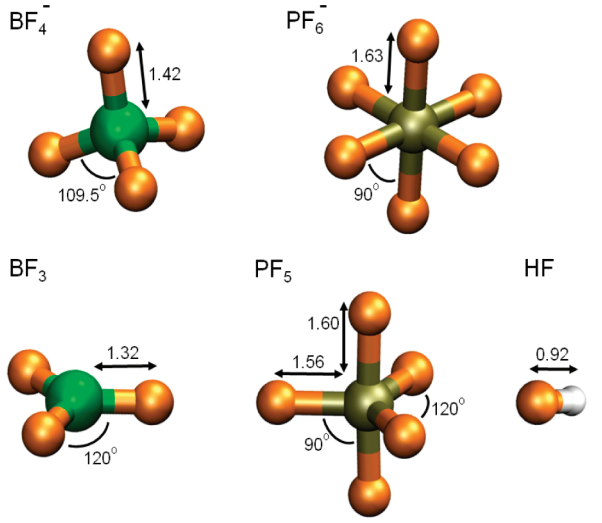

Figure 6. Structures of BF_4^-, PF_6^-, BF_3, PF_5, and HF in gas phase, as derived with the MP2/6-311++G(d,p) method. Distances are given in angstroms.

Table 7. Electronic Ground State Energy, Zero Point Vibrational Energy, Thermal Energy, Entropic Energy, and Free Energy of Various Compounds[a]

compound	E_0	E_{zp}	E_{therm}[b]	$-T\,S_{tot}$[b]	G[b,c]
BF_4^-	−423.7932	0.0140	0.0044	−0.0330	−423.8067
BF_3	−323.9842	0.0123	0.0035	−0.0306	−323.9979
PF_6^-	−939.1809	0.0189	0.0061	−0.0372	−939.1920
PF_5	−839.3542	0.0166	0.0055	−0.0362	−839.3672
HF	−100.2791	0.0096	0.0024	−0.0197	−100.2857
H^+	0	0	0.0014	−0.0124	−0.0100

[a] All values are given in atomic units. [b] T = 298 K was assumed for the calculation of these values. [c] The free energy of a compound is given by $G = E_0 + E_{zp} + E_{therm} + k_BT - TS_{tot}$

two anions are similar in their corresponding ILs, probably due to their similar size, geometry and coordination to the same cations. The solvation energies of neutral HF, BF_3 and PF_5 in the ILs are much smaller than for the anions, where HF is more favorably solvated than BF_3 and PF_5 due to the larger dipole moment.

3.4. Ground States of Anions and their Dissociated Conjugate Acids in Gas Phase. For the calculation of $\Delta\Delta G_0^{gas}$ in eq 7 the free energy of the isolated anions BF_4^- and PF_6^- as well as of their conjugate acids are required. As demonstrated in the previous section, the conjugate acids dissociate into HF and BF_3 or PF_5, which are the final stable product compounds of the proton transfer reaction. These compounds and the anions were treated with DFT as described in section 2.2 and their optimized structures are displayed in Figure 6. The corresponding free energies including the involved correction terms are given in Table 7. Values of $\Delta\Delta G_0^{gas}$ = 293.2 and 283.1 kcal/mol were derived for BF_4^- and PF_6^-, respectively. According to the definition of $\Delta\Delta G_0^{gas}$, the larger value in the case of BF_4^- suggests that this anion is a substantially stronger proton acceptor than PF_6^-, which agrees with experimental observations.[63]

3.5. Reaction Free Energies and pK_a Values of Tryptophan in ILs. The reaction free energy of proton transfer from $HTrp^+$ to the IL was determined with eq 7. All contributions and the final results are summarized in Table 8. Large increases of the reaction free energy for the proton transfer from Trp to the solvent of 19 and 26 kcal/mol were derived for BMIM-BF_4 and BMIM-PF_6, respectively. This means that the deprotonation of $HTrp^+$ is strongly impeded in both ILs compared to water. This reaction free energy change translated into a pK_a value for Trp of 21.5 in BMIM-PF_6 and 16.5 in BMIM-BF_4, compared to the well-known pK_a value of Trp in water of 2.4. For comparison, the acidity of $HTrp^+$ in BMIM-BF_4 is comparable to alcohols in water for instance. The statistical uncertainties of pK_a values were found to be only 0.3 units. This uncertainty, however, is expected to be smaller than the systematic errors caused by inevitable force field inaccuracies and the scaling of the solvation free energies. In any event, an examination of the single contributions to $\Delta\Delta G_0$ is necessary to elucidate the cause of the large pK_a shift.

Table 8. Contributions to Reaction Free Energy of Proton Transfer from $HTrp^+$ to Anions and pK_a Values of $HTrp^+$ in ILs[a,b,c]

	BMIM-PF_6	BMIM-BF_4
$\Delta\Delta G_{solv}^{HAA^+}$	-9.0_3	-4.4_3
$\Delta\Delta G_{solv}^{AA}$	-17.7_3	-15.1_3
$\Delta\Delta G_{solv}^{AN,IL}$	-36.5_2	-37.7_2
$\Delta\Delta G_0^{gas}$	+19.0	+29.1
$\Delta\Delta G_0$	-26.2_5	-19.3_5
ΔpK_a	-19.1_3	-14.1_3
pK_a	21.5_3	16.5_3

[a] All values are given in kcal/mol. [b] Statistical uncertainties of the last digit are given as subscripts. [c] Used symbols are defined in eqs 7−9.

The first term in eq 7, $\Delta\Delta G_{solv}^{HAA^+}$, was found to be −9 and −4 kcal/mol in BMIM-PF_6 and BMIM-BF_4, respectively. These values suggest that $HTrp^+$ is less favorably solvated in the two ILs, especially in BMIM-PF_6. An even stronger effect was observed in the case of Trp, where values of −18 and −15 kcal/mol for $\Delta\Delta G_{solv}^{AA}$ were obtained in BMIM-PF_6 and BMIM-BF_4, respectively. Also, the large values for $\Delta\Delta G_{solv}^{AN,IL}$ of about −37 kcal/mol in both ILs demonstrated how unfavorable the solvation of the neutral product compounds is compared to the solvation of the anions.

Compared with water, the negative values of the first two terms in eq 7 indicate that the reactant and product states in eq 4 are both destabilized by the IL due to the unfavorable solvation of Trp and $HTrp^+$. Since the effect is more pronounced in the case of Trp, the product state is more destabilized, thus the balance of the reaction is shifted toward the reactants. The third term in eq 7 shifts the balance even further toward the reactants because the solvation of an anion in the IL is much more favorable than of the neutral dissociated conjugate acid. The last term, $\Delta\Delta G_0^{gas}$, partially compensates these solvation effects, since the proton binds more favorably to the anions, especially to BF_4^-, than to a water complex around the proton that would be formed in water. In total, the protonated $HTrp^+$ state in eq 4 is stabilized relative to Trp, thus leading to the drastically increased pK_a values. In other words, deprotonation of $HTrp^+$ in ILs is massively impeded compared to that in water because it requires the annihilation of an anion and a cation in the reactant state, whose charges are stabilized by the ILs. We expect that these findings would apply qualitatively also to other deprotonation reactions of charged amino acids. The pK_a value of $HTrp^+$ is

dx.doi.org/10.1021/jp202486j |J. Phys. Chem. B 2011, 115, 8231–8241

substantially larger in BMIM-PF_6 than in BMIM-BF_4. Even though the solvation effects induced by the ILs are rather similar in the two cases, the difference was obtained due to the substantially different values of $\Delta\Delta G_0^{gas}$. The stabilizing effect of the product state through proton binding is diminished in the case of BMIM-PF_6 due to the reluctance of PF_6^- to accept protons. This is well illustrated by previously measured pK_a values of HBF_4 and HPF_6 in water, where values of −4.9 and −10 were obtained, respectively.[22,64]

The deprotonation of zwitterionic Trp was not considered in this work and is left for future work. However, a value can be readily estimated from the values in Table 8. The proton transfer reaction in this case is $Trp + AN^-(IL) \rightarrow Trp^- + X_1 + X_2(IL)$. This is similar to eq 4; that is, eq 7 can be used to estimate pK_a values when $HTrp^+$ is substituted with Trp and Trp with Trp^-. The contributions $\Delta\Delta G_0^{gas}$ and $\Delta\Delta G_{solv}^{AN,IL}$ in eq 7 do not depend on the amino acid and can be taken from previous calculations. Moreover, the solvation energies of Trp in water and ILs were already calculated as well. If we assume that the solvation energies of Trp^- in water and ILs are similar to the values for $HTrp^+$ in these solvents, the pK_a values can be estimated to 15.7 and 7.8 in BMIM-PF_6 and BMIM-BF_4, respectively, compared to 9.3 in water. The pK_a shifts are much smaller than in the case of $HTrp^+$ because the product state contains a charged Trp^-, which is stabilized by the ILs relative to the uncharged zwitterion.

The results of this work also help one understand the remarkable feature of ILs, in which proteins seem to memorize the pH of an aqueous solvent, where they had been solvated before. In other words, protein residues do not seem to change their protonation state upon solvation in ILs.[20] Four different proton transfer reactions between residues and pure IL could occur: (1) a positively charged residue transfers a proton to an anion; (2) a negatively charged residue accepts a proton from a cation; (3) an uncharged residue accepts a proton from a cation to become positively charged; (4) an uncharged residue donates a proton to an anion to become negatively charged. In the first two cases, two ions are annihilated in the reaction, which would lead to large positive pK_a shifts, as demonstrated. Thus, deprotonation of initially charged residues is highly unfavorable. In the latter two types of reactions, the number of ions in reactant and product state does not change, thus proton transfer should not be substantially impeded by solvation effects. In these cases, as discussed for the deprotonation of zwitterionic Trp, pK_a values of the residues in water could be used as rough estimates for the actual values in ILs. Cations in ILs are typically very weak acids (e.g., pK_a = 23 for dimethylimidazolium cations in water) and anions are very weak bases (e.g., pK_a = −4.9 for HBF_4 in water).[22,23] For the third reaction type, even the residue with the strongest proton affinity, arginine (pK_a = 12.1), could not abstract a proton from the more basic IL cations. For the forth reaction type, even the acidity of protonated aspartic acid (pK_a = 3.7), for instance, would be insufficient to protonate the more acidic anions in the IL. In summary, these considerations indeed suggest that in ILs a change in residue protonation is unlikely. Future further calculations and measurements are required to scrutinize these qualitative considerations.

4. CONCLUSION

The proton transfer reaction from $HTrp^+$ to anion constituents of the two ILs BMIM-PF_6 and BMIM-BF_4 was studied. A thermodynamic cycle was used that involved the calculation of solvation free energies of the reactant and product compounds in ILs with MD simulations. Additionally, the calculation of ground state free energies of these compounds in gas phase with DFT was included. It was observed in QM/MM MD simulations that protonated anions dissociated in ILs into HF and BF_3 or PF_5 molecules, which were treated as the product compounds of the reaction. On the basis of the results of this work, the reaction free energies for the proton transfer reactions in the ILs were determined relative to water and converted into pK_a values for $HTrp^+$ in ILs.

The resulting pK_a values of 21.5 in BMIM-PF_6 and 16.5 in BMIM-BF_4, respectively, are substantially larger than in water, indicating that the deprotonation of $HTrp^+$ is highly unfavorable in these pure ILs. Zwitterionic Trp is destabilized in both ILs compared to water. Even though charged $HTrp^+$ is also destabilized, this effect is partially compensated by favorable interactions of the additional charge with surrounding anions in the IL. Also the solvation of the product compounds BF_3, PF_5, and HF turned out to be very unfavorable compared to the solvation of the anions. Overall, the reaction balance was shifted toward $HTrp^+$ and anion in the reactant state compared to zwitterionic Trp, HF, and BF_3 or PF_5 in the product state due to the energetically unfavorable ion annihilation of one $HTrp^+$ and one anion per transferred proton. Even though solvation effects in BMIM-PF_6 and BMIM-BF_4 were found to be similar, the low basicity of PF_6^- compared to BF_4^- led to a substantially larger pK_a value of $HTrp^+$ in BMIM-PF_6.

We expect that these results can be generalized qualitatively to other proton transfer reactions between amino acids and pure ILs in which ions are annihilated. Estimates suggested that in proton transfer reactions where the number of ions remains the same, large pK_a shifts seem not to be induced by ILs. Further calculations are needed to clarify the variation of pK_a values upon modification of the ion constituents in the IL and upon variation of the amino acids. Furthermore, the effect of impurities in the IL, such as water, on pK_a values needs to be addressed in future work. In any event, for the first time, the pK_a values of amino acids in ILs were derived, and an explanation for the obtained large pK_a shifts was provided. Moreover, these results also contribute to elucidate the observed pH memory of proteins in ILs.

■ ASSOCIATED CONTENT

Supporting Information. The supporting material contains the solvation free energies of $HTrp^+$ in BMIM-PF_6 from simulations that contained only one solute as well as figures that display values of $\partial E/\partial\lambda$ as a function of λ for solutes solvated in ILs and water. This information is available free of charge via the Internet at http://pubs.acs.org/.

■ AUTHOR INFORMATION

Corresponding Author

*Phone: (65) 6419 1468. Fax: (65) 6463 2536. E-mail: marco@ihpc.a-star.edu.sg.

■ ACKNOWLEDGMENT

We gratefully acknowledge the allocation of computational resources by the Institute of High Performance Computing and the Advanced Computing Resource Center in Singapore as well as the financial support from the Agency for Science, Technology and

Research of Singapore. Furthermore, we like to thank Jan Bitenc and Matic Pavlin from the University of Ljubljana, Slovenia, for their valuable contributions to this work.

REFERENCES

(1) Weingärtner, H. *Angew. Chem., Int. Ed.* **2008**, *47*, 654–670.
(2) Wasserscheid, P.; Welton, T. *Ionic Liquids in Synthesis*; Wiley-VCH: Weinheim, Germany, 2003.
(3) Seddon, K. R. *Nat. Mater.* **2003**, *2*, 363–365.
(4) Welton, T. *Chem. Rev.* **1999**, *99*, 2071–2083.
(5) Rogers, R. D.; Seddon, K. R. *Science* **2003**, *302*, 792–793.
(6) Lau, R. M.; van Rantwijk, F.; Seddon, K. R.; Sheldon, R. A. *Org. Lett.* **2000**, *2*, 4189–4191.
(7) Schmid, A.; Dordick, J. S.; Hauer, B.; Kiener, A.; Wubbolts, M.; Witholt, B. *Nature* **2001**, *409*, 258–268.
(8) van Rantwijk, F.; Sheldon, R. A. *Chem. Rev.* **2007**, *107*, 2757–2785.
(9) Fujita, K.; MacFarlane, D. R.; Forsyth, M. *Chem. Commun.* **2005**, 4804–4806.
(10) Majewski, P.; Pernak, A.; Grzymislawski, M.; Iwanik, K.; Pernak, J. *Acta Histochem.* **2003**, *105*, 135–142.
(11) Xiong, H. Y.; Chen, T.; Zhang, X. H.; Wang, S. F. *Electrochem. Commun.* **2007**, *9*, 1648–1654.
(12) Huddleston, J. G.; Willauer, H. W.; Swatloski, R. P.; Visser, A. E.; Rogers, R. D. *Chem. Commun.* **1998**, *16*, 1765–1766.
(13) Cull, S. G.; Holbrey, J. D.; Vargas-Mora, V.; Seddon, K. R.; Lye, G. J. *Biotechnol. Bioeng.* **2000**, *69*, 227–233.
(14) Fadeev, A. G.; Meagher, M. M. *Chem. Commun.* **2001**, 295–296.
(15) Wang, J.; Pei, Y.; Zhao, Y.; Hu, Z. *Green Chem.* **2005**, *7*, 196–202.
(16) Shimojo, K.; Nakashima, K.; Kamiya, N.; Goto, M. *Biomacromolecules* **2006**, *7*, 2–5.
(17) Thomas, P. G.; Russel, A. J. F., A. R. *Nature* **1985**, *318*, 375–376.
(18) Becktel, W. J.; Schellman, J. A. *Biopolymers* **1987**, *26*, 1859–1877.
(19) Vicatos, S.; Roca, M.; Warshel, A. *Proteins* **2009**, *77*, 670–984.
(20) Ren, M. Y.; Bai, S.; Zhang, D. H.; Sun, Y. *J. Agr. Food Chem.* **2008**, *56*, 2388–2391.
(21) Malham, I. B.; Letellier, P.; Turmine, M. *Talanta* **2008**, *77*, 48–52.
(22) Papcun, J. R. Fluorine Compounds, Inorganic, Fluoroboric Acid and Fluoroborates. In *Kirk-Othmer Encyclopedia of Chemical Technology*; John Wiley & Sons, Inc.: New York, 2000.
(23) Amyes, T. L.; Diver, S. T.; Richard, J. P.; Rivas, F. M.; Toth, K. *J. Am. Chem. Soc.* **2004**, *126*, 4366–4374.
(24) Thomazeau, C.; Olivier-Bourbigou, H.; Magna, L.; Luts, S.; Gilbert, B. *J. Am. Chem. Soc.* **2003**, *125*, 5264–5265.
(25) D'Anna, F.; Marullo, S.; Vitale, P.; Noto, R. *J. Org. Chem.* **2010**, *75*, 4828–4834.
(26) Klähn, M.; Stüber, C.; Seduraman, A.; Wu, P. *J. Phys. Chem. B* **2010**, *114*, 2856–2868.
(27) Tome, L. I. N.; Catambas, V. R.; Teles, A. R. R.; Freire, M. G.; Marrucho, I. M.; Coutinho, J. A. P. *Sep. Purif. Technol.* **2010**, *72*, 167–173.
(28) Acevedo, O.; Jorgensen, W. L.; Evanseck, J. *J. Chem. Theory Comput.* **2007**, *3*, 132–138.
(29) Sambasivarao, S. V.; Acevedo, O. *J. Chem. Theory Comput.* **2009**, *5*, 1038–1050.
(30) Arantes, G. M.; Ribeiro, M. C. C. *J. Chem. Phys.* **2008**, *128*, 114503.
(31) Yockel, S.; Schatz, G. C. *J. Phys. Chem. B* **2010**, *114*, 14241–14248.
(32) Frisch, M. J.; Trucks, G. W.; Schlegel, H. B.; Scuseria, G. E.; Robb, M. A.; Cheeseman, J. R.; Montgomery, J.; J. A.; Vreven, T.; Kudin, K. N.; Burant, J. C. et al. *Gaussian 03*, revision C.02; Gaussian, Inc.: Wallingford, CT, 2004.
(33) Head-Gordon, M.; Pople, J. A.; Frisch, M. J. *Chem. Phys. Lett.* **1988**, *153*, 503–506.
(34) McQuarrie, D. A. *Molecular Thermodynamics*; University Science Books: Sausalito, CA, 1999.
(35) Van der Spoel, D.; Lindahl, E.; Hess, B.; Groenhof, G.; Mark, A. E.; Berendsen, H. J. C. *J. Comput. Chem.* **2005**, *26*, 1701–1718.
(36) Beutler, T. C.; Mark, A. E.; van Schaik, R. C.; Gerber, P. R.; van Gunsteren, W. F. *Chem. Phys. Lett.* **1994**, *222*, 529–539.
(37) Hess, B. *J. Chem. Phys.* **2002**, *116*, 209–217.
(38) Klähn, M.; Seduraman, A.; Wu, P. *J. Phys. Chem. B* **2008**, *112*, 10989–11004.
(39) Lopes, J. N. C.; Padua, A. A. H.; Shimizu, K. *J. Phys. Chem. B* **2008**, *112*, 5039–5046.
(40) Becke, A. D. *J. Chem. Phys.* **1993**, *98*, 5648–5652.
(41) Lee, C. T.; Yang, W. T.; Parr, R. G. *Phys. Rev. B* **1988**, *37*, 785–789.
(42) Field, M. J.; Bash, P. A.; Karplus, M. *J. Comput. Chem.* **1990**, *11*, 700–733.
(43) Breneman, C. M.; Wiberg, K. B. *J. Comput. Chem.* **1990**, *11*, 361–373.
(44) Duan, Y.; Wu, C.; Chowdhury, S.; Lee, M. C.; Xiong, G.; Zhang, W.; Yang, R.; Cieplak, P.; Luo, R.; Lee, T.; et al. *J. Comput. Chem.* **2003**, *24*, 1999–2012.
(45) Tomasi, J.; Mennucci, B.; Cammi, R. *Chem. Rev.* **2005**, *105*, 2999–3093.
(46) Mahoney, M. W.; Jorgensen, W. L. *J. Chem. Phys.* **2000**, *112*, 8910–8922.
(47) Mahoney, M. W.; Jorgensen, W. L. *J. Chem. Phys.* **2001**, *114*, 363–366.
(48) Allen, M. P.; Tildesley, D. J. *Computer Simulations of Liquids*; Oxford Science Publications: Oxford, 1987.
(49) Darden, T.; York, D.; Pedersen, L. *J. Chem. Phys.* **1993**, *98*, 10089–10092.
(50) Essmann, U.; Perera, L.; Berkowitz, M. L.; Darden, T.; Lee, H.; Pedersen, L. G. *J. Chem. Phys.* **1995**, *103*, 8577–8593.
(51) Bussi, G.; Donadio, D.; Parrinello, M. *J. Chem. Phys.* **2007**, *126*, 014101.
(52) Berendsen, H. J. C.; Postma, J. P. M.; DiNola, A.; Haak, J. R. *J. Chem. Phys.* **1984**, *81*, 3684–3690.
(53) Eichinger, M.; Tavan, P.; Hutter, J.; Parrinello, M. *J. Chem. Phys.* **1999**, *110*, 10452–10467.
(54) Chang, J.; Lenhoff, A. M.; Sandler, S. I. *J. Phys. Chem. B* **2007**, *111*, 2098–2106.
(55) Vohringer-Martinez, E.; Toro-Labbe, A. *J. Phys. Chem. B* **2010**, *114*, 13005–13010.
(56) Jorgensen, W. L.; Maxwell, D. S.; Tirado-Rives, J. *J. Am. Chem. Soc.* **1996**, *118*, 11225–11236.
(57) Perdan-Pirkmajer, K.; Mavri, J.; Krzan, M. *J. Mol. Model* **2010**, *16*, 1151–1158.
(58) Tissandier, M. D.; Cowen, K. A.; Feng, W. Y.; Gundlach, E.; Cohen, M. H.; Earhart, A. D. *J. Phys. Chem. A* **1998**, *102*, 7787–7794.
(59) Kelly, C. P.; Cramer, C. J.; Truhlar, D. G. *J. Phys. Chem. B* **2006**, *110*, 16066–16081.
(60) Anthony, J. L.; Maginn, E. J.; Brennecke, J. F. *J. Phys. Chem. B* **2001**, *105*, 10942–10949.
(61) Freire, M. G.; Neves, C. M. S. S.; Carvalho, P. J.; Gardas, R. L.; Fernandes, A. M.; Marrucho, I. M.; Santos, L. M. N. B. F.; Coutinho, J. A. P. *J. Phys. Chem. B* **2007**, *111*, 13082–13089.
(62) Klähn, M.; Lim, G. S.; Seduraman, A.; Wu, P. *Phys. Chem. Chem. Phys.* **2011**, *13*, 1649–1662.
(63) Kazarian, S. G.; Briscoe, B. J.; Welton, T. *Chem. Commun.* **2000**, 2047–2048.
(64) Hirano, M.; Kuga, T.; Kitamura, M.; Kanaya, S.; Komine, N.; Komiya, S. *Organometallics* **2008**, *27*, 3635–3638.